Research Article

Space-Time-Frequency Characterization of 3D Nonisotropic MIMO Multicarrier Propagation Channels Employing Directional Antennas

Hamidreza Saligheh Rad[1] and Saeed Gazor[2]

[1] *School of Engineering and Applied Sciences, Harvard University, Cambridge, MA 02138, USA*
[2] *Department of Electrical and Computer Engineering, Queen's University, Kingston, ON, Canada K7L 3N6*

Correspondence should be addressed to Hamidreza Saligheh Rad, hamid@seas.harvard.edu

Channel models for outdoor wireless systems usually assume two-dimensional (2D) random scattering media. In the practical outdoor wireless channels, the impact of the wave propagation in the third-dimension is definitely important; especially when the communication system efficiently exploits potentials of multiple antennas. In this paper, we propose a new model for multiple-input multiple-output (MIMO) multicarrier propagation channels in a three-dimensional (3D) environment. Specifically, the proposed model describes the cross-correlation function (CCF) between two subchannels of an outdoor MIMO channel employing directional antennas and in the presence of nonisotropic wave propagation in 3D space. The derived CCF consists of some correlation terms. Each correlation term is in the form of a linear series expansion of averaged Bessel functions of the first kind with different orders. In practice, each correlation term has a limited number of Bessel components. Our numerical evaluations show the impact of different parameters of the propagation environment as well as the employed antennas on the resulting CCF. Using the proposed CCF, we also establish simple formulas to approximate the coherence time, the coherence bandwidth and the spatial coherence of such channels. The numerical curve fitting results fit to the empirical results reported in the channel modeling literature.

1. INTRODUCTION

Space-time-frequency (STF) models are required to realistically evaluate the performance and to comprehensively understand the behavior of multiple-input multiple-output (MIMO) multicarrier communication systems in the presence of fading(s) [1]. Most of existing MIMO models for outdoor environments assume wave propagation in a two-dimensional (2D) horizontal space, considering a *special geometry* for the scatterers combined with appropriate probability density functions (pdfs) for the physical parameters, for example, [2, 3]. On the other hand, outdoor wireless channels are significantly influenced by nonisotropic distribution of scatterers in the propagation environment, the response of the employed antennas as well as the direction

and the speed of the mobile station (MS). This paper is motivated in order to consider the following:

   (i) the impact of the wave propagation in a three-dimensional (3D) nonisotropic environment without employing any specific geometry for randomly distributed scatterers in the space;

  (ii) the impact of 3D directional antennas at both transmitter and receiver arrays;

 (iii) the impact of multicarrier communication in a MIMO system.

We introduce an STF cross-correlation function (CCF) for two subchannels of a MIMO multicarrier wireless channel, that is, of two pairs of antenna elements, two time indices and at two carrier frequencies.

The calculation of the CCF for a 3D-MIMO propagation environment has attracted the attention of several researchers, for example, [4–10]. Mohasseb and Fitz in [4] propose a 3D generalization of the Clarke/Jake's model [11] for a MIMO system. The model considers the famous one-ring geometry for the distribution of scatterers. Abhayapala et al., develop a 3D spatial channel model to provide insight into spatial aspects of multiple antenna communication systems [5]. Yong and Thompson derive a closed-form expression of the spatial fading correlation function employing a uniform rectangular array in a 3D multipath channel [6]. Yao and Pätzold investigate the spatial-temporal characteristics of a 3D theoretical channel model for scatterers that form a half-spheroid with a given axial length ratio [7]. Using a 3D cylinder scattering model (specific geometry for the distribution of scatterers), Leong et al. in [8] propose a closed-form formula for the space-time correlation function for MIMO systems. Özdemir et al. suggest a model to combine improved sum-of-sinusoids simulation models proposed for fading channels, and the 2D models proposed for MIMO systems, in a 3D scattering environment [9]. The distribution of 3D scattering is uniform in horizontal plane and Gaussian in the elevated plane. Teal et al. generalize the well-known results of the spatial correlation function for two-dimensional and three-dimensional diffuse fields of narrowband signals to the case of general distributions of scatterers [10].

As a summary, our literature review shows that available CCFs for 3D-MIMO outdoor environments are mostly based on specific geometries of scatterers in the space and therefore, each model is just capable to predict the behavior of that particular propagation scenario. Moreover, they are not able to investigate the spatial, the temporal, and the frequency aspects of the wireless channel in one single model. In this paper, we propose a framework to calculate the STF-CCF for MIMO multicarrier (e.g., orthogonal frequency division multiplexing) channels for a class of 3D outdoor propagation environments. In contrast to some recent works, we do not assume a special geometry to describe the relative position/distribution of scatterers in the space. Besides, we assume that the direction of arrivals (to the receiver) and the direction of departures (from the transmitter) are independent. This assumption is a sufficient condition—and not necessary—for our model to be valid, and represents the class of microcell urban propagation environments. We employ the Fourier series expansion (FSE) of pdfs of the nonisotropic azimuth angle spread (AAS) and the nonisotropic elevation angle spread (EAS) for both MS and base station (BS) sides. Measurements for outdoor environments show that the AAS is either truncated Laplacian or truncated Normally distributed [12–14]. In addition, we introduce a class of pdfs for the EAS as a basis such that any arbitrary (isotropic or nonisotropic) EAS can be represented by a convex linear combination of members of this class. By this means, the CCF is represented as the same linear combination of CCFs associated to these pdfs. This allows accurate modeling for various 3D wireless propagation environments. We use the Fourier series coefficients (FSCs) of 3D antenna propagation patterns (APPs) to investigate the impact of directional

antennas in this model. We extensively evaluate the behavior of the CCF in terms of the propagation environment, the employed antennas as well as the direction and the speed of the MS in both time and frequency domains.

In Section 2, the assumptions on the parameters of the propagation medium and the employed antennas are described. The proposed CCF is calculated in Section 3. Numerical analysis on the derived CCF is proposed in Section 4. This includes the Fourier analysis of the CCF to result in the channel power spectrum, the coherence-time (CT), and the coherence-bandwidth (CB) in different circumstances. The discussions and conclusions are brought together in Section 5.

2. THREE-DIMENSIONAL MIMO MODEL DESCRIPTION

Figure 1 shows a pair of BS-MS antennas from a multielement communication system in a 3D propagation environment. The figure shows the coordinates of the moving MS and the fixed BS. This figure also shows the elevation and the azimuth angles in either the BS or the MS coordinates. The following are the employed notations throughout the paper.

(i) O^B, O^M: BS coordinate, MS coordinate;

(ii) $h_{pm}(t, \omega)$: channel TF between pth BS antenna element and mth MS antenna element;

(iii) $\mathbf{a}_p^B$: position vector of the pth antenna element on the BS side relative to O^B;

(iv) $\mathbf{a}_m^M$: position vector of the mth antenna element on the MS side relative to O^M;

(v) $\boldsymbol{\Psi}_i^B$: the unity vector pointing to the direction-of-departure (DOD) of the ith path from the BS;

(vi) $\boldsymbol{\Psi}_i^M$: the unity vector pointing to the direction-of-arrival (DOA) of the ith path to the MS;

(vii) Θ_i^B; Θ_i^M: the DOD azimuthal angle from the BS; the DOA azimuthal angle to the MS;

(viii) Ω_i^B; Ω_i^M: the DOD elevation angle from the BS; the DOA elevation angle to the MS;

(ix) $G_p^B(\Theta^B, \Omega^B; \omega)$: antenna propagation pattern of the pth antenna element of the BS array;

(x) $G_m^M(\Theta^M, \Omega^M; \omega)$: antenna propagation pattern of the mth antenna element of the MS array;

(xi) $\mathbf{v}$; c: MS speed vector; wave propagation velocity;

(xii) $\tau_{p,m;i}$: delay between pth BS antenna element and mth MS antenna element via ith path;

(xiii) $g_{p,m;i}$: gain between pth BS and mth MS antenna elements via the ith path, approximated by g_i;

(xiv) ϕ_i; ω: phase contribution along the ith path; carrier frequency;

(xv) $\overline{\tau}$; σ: mean and delay spread of the time-delay distribution function τ_i;

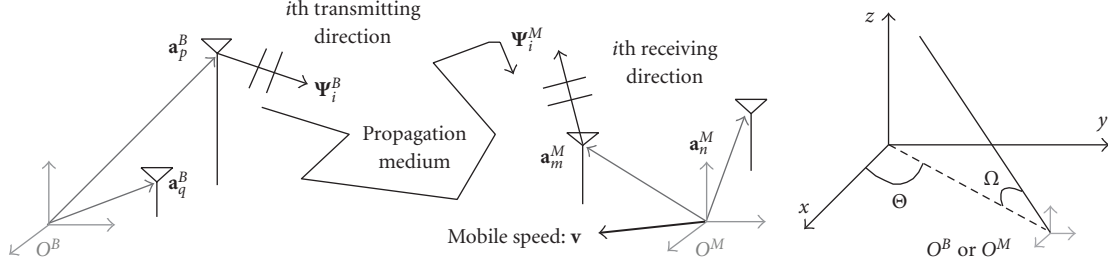(xvi) η; I: pathloss exponent; number of total paths.

FIGURE 1: *3D space.* One pair of BS-MS antennas in the 3D space: pth (qth) antenna element of BS and mth (nth) antenna element of MS in their local coordinate axis in a 3D wave propagation environment. Azimuth and elevation angles in the 3D propagation environment.

Superscripts B and M indicate variables at the BS and the MS sides, respectively; vectors are bolded lowercased letters or bolded Roman letters, and $(\cdot)^T$ represents the transpose operation. One should note that here we have $\mathbf{\Psi}_i \triangleq [\cos(\Omega_i)\cos(\Theta_i), \cos(\Omega_i)\sin(\Theta_i), \sin(\Omega_i)]^T$ [15]. In the multipath propagation environment, the received signal is composed of a linear combination of plane waves where each received waveform (the ith received waveform) is associated with a path attenuation gain $g_{p,m;i}$, a path phase shift ϕ_i, a time-varying delay $\tau_{p,m;i}(t)$, and a complex gain composed of the antenna patterns at both BS and MS $G_p^B(\Theta_i^B, \Omega_i^B; \omega)G_m^M(\Theta_i^M, \Omega_i^M; \omega)$. The APPs $G_p^B(\Theta_i^B, \Omega_i^B; \omega)$ and $G_m^M(\Theta_i^M, \Omega_i^M; \omega)$ are known functions in terms of the propagation directions and the carrier frequency. The channel transfer-function (CTF) of each subchannel consisting of the transmitting antenna element located at $\mathbf{a}_p^B$, the propagation environment, and the receiving antenna element located at $\mathbf{m}_m^M$ is given by

$$h_{pm}(t,\omega) \triangleq \sum_{i=1}^{I} G_p^B(\Theta_i^B, \Omega_i^B; \omega)G_m^M(\Theta_i^M, \Omega_i^M; \omega)g_{p,m;i} \times \exp\left(j\phi_i - j\omega\tau_{p,m;i}(t)\right), \quad (1)$$

where I is the number of mutipath waveforms resulting from scattering. The CTF, $h_{pm}(t,\omega)$, is defined as the gain between baseband representation of the input and the output of the channel assuming that the bandwidth of the transmitted signal is smaller than the channel bandwidth (see [2, 16] for more information). The propagation delay over the ith path, $\tau_{p,m;i}(t) \triangleq \tau_{p,m;i} - (t/c)\mathbf{v}^T\mathbf{\Psi}_i^M$, is time-varying due to the mobility of the MS. Substituting the time-varying delay in (1), the CTF of such a propagation environment is represented by

$$h_{pm}(t,\omega) = \sum_{i=1}^{I} G_p^B(\Theta_i^B, \Omega_i^B; \omega)G_m^M(\Theta_i^M, \Omega_i^M; \omega)g_{p,m;i} \times \exp\left(j\phi_i + j\varpi_i t - j\omega\tau_{p,m;i}\right), \quad (2)$$

where the shifted frequency of the ith received waveform caused by the Doppler effect is denoted by the Doppler shift $\varpi_i \triangleq (\omega/c)\mathbf{v}^T\mathbf{\Psi}_i^M$, ω is the carrier frequency, and $\mathbf{v}$ and c are the MS velocity vector and the speed of light, respectively. We make the following further assumptions.

(A1) We assume that the distance between scatterers and antenna arrays is much larger than the interelement antenna distances. Therefore, propagation waveforms in the scattering environment are plane waves and there is no interelement scattering. We also assume that the number of propagation paths is large enough such that the channel is Rayleigh by virtue of the central limit theorem [16]. The transmitted signal travels between the MS and the BS, from each transmitting antenna to each receiving antenna. The signal travels through the media via a number of multipath waveforms with different lengths. Here, we assume no line-of-sight, however, the line-of-sight propagation path between the transmitter and the receiver can be separately treated [2, 17].

(A2) The pdfs of the azimuth propagation directions, $f_A^B(\Theta^B)$ and $f_A^M(\Theta^M)$ over $[-\pi, \pi)$, characterize the non-isotropic propagation environment in the 2D azimuthal plane. Since these density functions are periodic functions with period 2π, we represent them by their FSE pairs as follows:

$$\mathcal{F}_{A;k}^B \longleftrightarrow f_A^B(\Theta^B), \qquad \mathcal{F}_{A;k}^M \longleftrightarrow f_A^M(\Theta^M), \quad (3a)$$

$$\mathcal{F}_{A;k} = \frac{1}{2\pi}\int_{-\pi}^{\pi} f_A(\Theta)e^{-jk\Theta}d\Theta, \qquad f_A(\Theta) = \sum_{k=-\infty}^{+\infty} \mathcal{F}_{A;k}e^{jk\Theta}. \quad (3b)$$

Reported measurement results suggest two candidates for these pdfs, namely, truncated-Normal and truncated-Laplace distributions [12–14]. In [18], authors give a complete investigation on these distributions and their FSEs.

(A3) The pdfs of the elevation propagation directions, $f_E^B(\Theta^B)$ and $f_E^M(\Theta^M)$ over $[-\pi, \pi)$, characterize the non-isotropic propagation environment in the elevation. Similarly, we use their FSE pairs as follows:

$$\mathcal{F}_{E;k}^B \longleftrightarrow f_E^B(\Omega^B), \qquad \mathcal{F}_{E;k}^M \longleftrightarrow f_E^M(\Omega^M), \quad (4a)$$

$$\mathcal{F}_{E;k} = \frac{1}{2\pi}\int_{-\pi}^{\pi} f_E(\Omega)e^{-jk\Omega}d\Omega, \qquad f_E(\Omega) = \sum_{k=-\infty}^{+\infty} \mathcal{F}_{E;k}e^{jk\Omega}. \quad (4b)$$

For simplicity of expressions, EAS pdfs are defined over $[-\pi, \pi)$ while they are nonzero only in the range of $[-\pi/2, \pi/2]$. The distribution of the EAS follows independent and identically distributed (i.i.d.) random variables. It

is clear that the majority of incoming/outgoing waves do travel in nearly horizontal directions. The determination of the EAS of such waves requires some considerations, as it depends on the environmental parameters like the degree of urbanization [19]. This determination has attracted the attention of some theoretical/experimental researchers [19–23]. Aulin in [20] and Parsons and Turkmani in [19] suggest realistic pdfs for EAS in a microcellular environment. These pdfs do not result in closed-form or easy-to-use expressions for the CCF in the case of MIMO systems. Qu and Yeap in [21] suggest a family of pdfs with two parameters for both symmetrical and asymmetrical pdfs of the EAS. Kuchar et al. in [22] measure the power angle spectrum at the MS in downtown Paris at 890 MHz. According to this work, propagation over the roofs is significant; typically 65% of energy is incident with an elevation larger than 10°. Kalliola et al. measure the EAS distribution at an MS in different radio propagation environments at 2.15 GHz [23]. Results show that in non-LOS situations, the power distribution in elevation has the shape of a double-sided exponential function, with different slopes on the negative and the positive sides of the peak. The slopes and the peak elevation angle depend on the environment and the BS antenna height. In order to satisfy the requirements of a pdf for realistic EAS previously proposed in the literature, we consider a family of distributions for $|\Omega| \leq \pi/2$ ($f_E(\Omega) = 0$, $|\Omega| > \pi/2$) as follows [10, 24]:

$$\text{EAS I:} \quad f_E(\Omega) = \frac{\Gamma(\alpha+1)\cos^{2\alpha}(\Omega)}{\sqrt{\pi}\Gamma(\alpha+1/2)}, \tag{5a}$$

$$\text{EAS II:} \quad f_E(\Omega) = \frac{2\left|\sin(\Omega)\right|^{2\alpha}\cos(\Omega)}{2\alpha+1}, \tag{5b}$$

where $\Gamma(u) = \int_0^\infty \xi^{u-1}e^{-\xi}d\xi$ is the Gamma function [15, page 258], and $\alpha \geq 0$ is related to the degree of urbanization. The parameter α specifies the type of the environment in the sense of how many waves are scattered into the third dimension of the space; the larger α, the more waves scattered into the third dimension. In another words, larger values for α characterize more urban environments in which more multipath waves are propagated into the third dimension. Interestingly, a linear convex combination of the members of this class as a pdf covers a wide class of distributions that is able to realistically model a nonisotropic environment in the third dimension. Empirical data taken from real measurement scenarios are needed to calculate the coefficients of this linear combination. After the pdf of the EAS is approximated, it is then expanded into its series of FSCs in order to substitute the resulting pdf with its equivalent FSE. Therefore, it is possible to substitute the infinite series of FSCs with a limited number of coefficients to the extent that it holds a certain level of accuracy to represent the original pdf. Figure 2 compares the FSCs of the suggested pdfs in two cases: EAS I and EAS II, and for different values of α. Simulations results show that when the value of α increases, the necessary number of FSCs to reconstruct the EAS distribution increases.

(A4) The complex APPs of the pth antenna at the BS and the mth antenna at the MS and in the carrier frequency ω, $G_p^B(\Theta^B, \Omega^B; \omega)$ and $G_m^M(\Theta^M, \Omega^M; \omega)$, give the response of antenna elements in terms of the azimuth and the elevation propagation directions and the carrier frequency. These pattern functions are periodic functions in terms of Θ and Ω with the period 2π, therefore, we represent them by their FSE pairs as follows:

$$G(\Theta, \Omega; \omega),$$
$$\mathcal{G}_{k_1,k_2}(\omega) = \frac{1}{4\pi^2}\int\int_{-\pi}^{\pi} G(\Theta, \Omega; \omega)e^{-jk_1\Theta}e^{-jk_2\Omega}d\Theta \, d\Omega, \tag{6a}$$

$$G(\Theta, \Omega; \omega) = \sum_{k_1=-\infty}^{+\infty}\sum_{k_2=-\infty}^{+\infty}\mathcal{G}_{k_1,k_2}(\omega)e^{jk_1\Theta}e^{jk_2\Omega}. \tag{6b}$$

For simplicity, APPs in the third dimension and for the parameter Ω are defined over $[-\pi, \pi)$, while they are periodic with fundamental period of π. 3D-APPs of two commonly used antennas in wireless applications are as follows ($\Theta \in [-\pi, \pi)$, $\Omega \in [-\pi, \pi)$ [25]):

half-wavelength dipole:

$$G(\Theta, \Omega; \omega) = G_0 j \frac{\cos((\pi/2)\cos\Theta)\sin((\omega/c)h\sin\Theta\cos\Omega)}{\sin\Theta\sin((\omega/2c)h\sin\Theta\cos\Omega)}; \tag{7a}$$

horizontal electric dipole:

$$G(\Theta, \Omega; \omega) = G_0 j\sqrt{1 - \sin^2\Theta\sin^2\Omega}\sin\left(\frac{\omega}{c}h\cos\Theta\right), \tag{7b}$$

where h is proportional to the size of the antenna and G_0 is the real and positive constant antenna gain that varies for each antenna. We note that an omnidirectional antenna is represented by a constant APP, that is, $G(\Theta, \Omega; \omega) = G_0$. Figure 3 shows the absolute value of the FSCs of these APPs, where $h = c/2f$ and the carrier frequency of $\omega = 2\pi f$. We observe that for these antennas, the value of $\mathcal{G}_{k_1,k_2}$ is considerable only for a limited number of coefficients. Also, we usually need more coefficients when the size of the antenna increases. One should note that the horizontal electric dipole needs more number of coefficients to precisely construct the related APP.

(A5) We decompose the ith path propagation delay, $\tau_{p,m;i}$, into three components: one major delay because of the distance between BS and MS, and two relative propagation delays with respect to local coordinates across BS and MS antenna arrays, as follows:

$$\tau_{p,m;i} = \tau_i - \left(\tau_{p;i}^B + \tau_{m;i}^M\right), \tag{8a}$$

$$\tau_{p;i}^B \triangleq \frac{\mathbf{a}_p^{B^T}\mathbf{\Psi}_i^B}{c}, \quad \tau_{m;i}^M \triangleq \frac{\mathbf{a}_m^{M^T}\mathbf{\Psi}_i^M}{c}, \tag{8b}$$

where $(\cdot)^T$ represents the transpose operator, τ_i represents the delay between O^B and O^M, and $\tau_{p;i}^B$ and $\tau_{m;i}^M$ represent relative propagation delays from antenna elements, $\mathbf{a}_p^B$ or $\mathbf{a}_m^M$, to corresponding coordinates, O^B or O^M, respectively [17]. We must note that the propagation delay and the Doppler shift for each individual multipath component are functions of DOA and/or DOD, and hence they may be
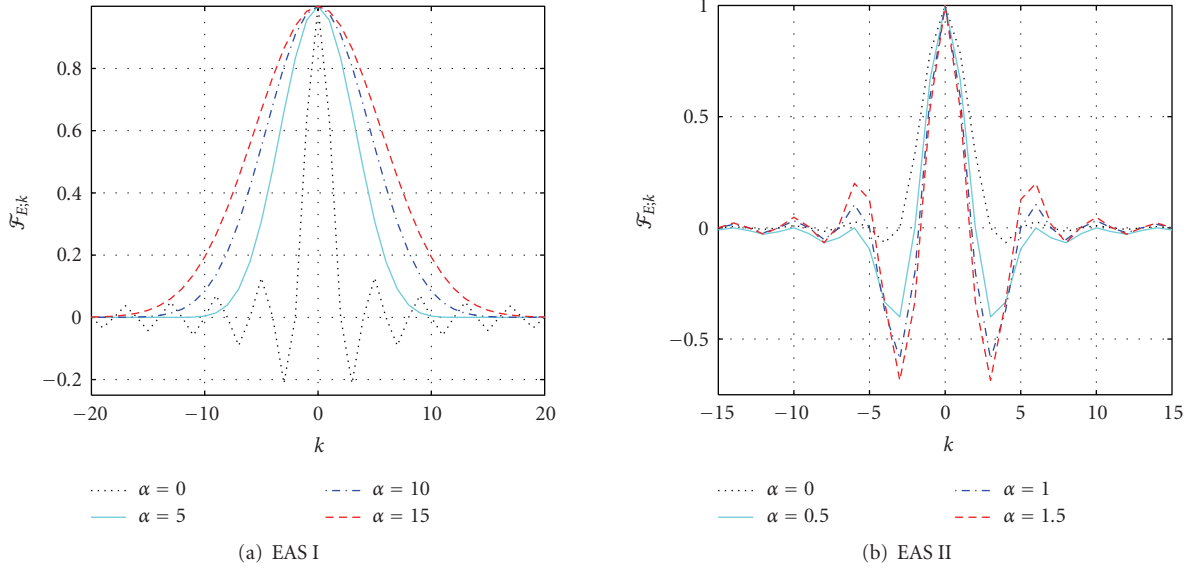
FIGURE 2: *Fourier series coefficients of different suggested elevation pdfs (EASs), in two different propagation environments: (a) EAS I and (b) EAS II. Different environments are specified by different values of the degree of urbanization α.*
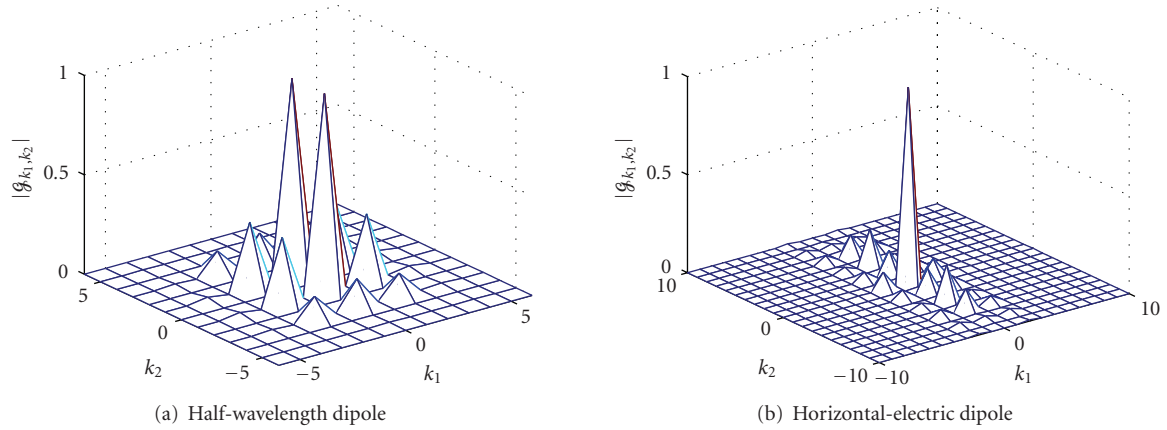

FIGURE 3: *Normalized Fourier series coefficients,* $|\mathscr{G}_{k_1,k_2}|/\max_{l_1,l_2}|\mathscr{G}_{l_1,l_2}|$, *for* $h = c/2f$ *and (a) half-wavelength dipole, (b) horizontal-electric dipole.*

dependent. However in this work, the major delay τ_i is assumed to be independent of DOA and/or DOD, and therefore, it is also independent from the Doppler spread. Relative large and random displacements of scatterers may make this assumption invalid. The impact of the random displacements of scatterers is investigated in [26]. In outdoor propagation environments, the time-delays τ_i are commonly assumed to be i.i.d. random variables which are exponentially distributed [3, 16]. The distribution of the time-delay τ_i is $f_{\tau_i}(x) = (1/\sigma)e^{-(x-\bar{\tau}+\sigma)/\sigma}$, for all $x \geq \bar{\tau} - \sigma$, where $\bar{\tau} = E[\tau_i]$ is the mean value to specify the distance (major propagation distance) between the MS and the BS, and σ is the delay spread. The moment generating function (MGF) of the time-delay pdf is given by $\Phi_\tau(s) = e^{(\bar{\tau}-\sigma)s}/(1 - \sigma s)$. Given a random variable x with the pdf $f_X(x)$, the MGF of this random variable is defined as follows: $\Phi_X(s) = E[e^{jsX}] = \int_{-\infty}^{+\infty} e^{js\xi} f_X(\xi)d\xi$.

(A6) Assuming $|\tau_i| \gg \max\{|\tau_{p;i}^B|, |\tau_{m;i}^M|\}$, the path-gain as a function of the time delay will be

$$g_{p,m;i} \simeq g_i = \sqrt{\frac{P}{I}} \tau_i^{-\eta/2}, \qquad (9)$$

where η is the pathloss exponent, I is the number of propagation paths, and P is a normalization constant [27–29]. Pathloss exponent is usually a function of carrier frequency, and parameters of the propagation medium such as obstructions. For example, around 1 GHz, it typically ranges from 2 to 8. The term $1/\sqrt{I}$ is introduced to retain a constant power random process. The appropriate (and approximate) value for the pathloss exponent is $\eta = 2$ for free-space propagation, $\eta = 4$ for rural and $\eta = 6$ for crowded urban environments [17, 27].

(A7) As a consequence of the planar wave propagation, the path phase shift ϕ_i accurately approximates $\phi_{p,m;i}$. We take into account the phase contribution of scatterers by uncorrelated random phase changes $\phi_i \sim U[-\pi, \pi]$.

3. THREE-DIMENSIONAL SPACE-TIME-FREQUENCY CROSS-CORRELATION FUNCTION

Using the above assumptions, we derive an expression for the STF-CCF between CTFs of two arbitrary MIMO subchannels, $h_{pm}(t, \omega)$ and $h_{qn}(t, \omega)$. This CCF is denoted by

$$R_{pm,qn}(t_1, t_2; \omega_1, \omega_2) \triangleq E[h_{pm}(t_1, \omega_1) h_{qn}^*(t_2, \omega_2)], \quad (10)$$

and is a function of sampling times (t_1, t_2), carrier frequencies (ω_1, ω_2), and antenna elements $(m, p; n, q)$. We rewrite the CCF by replacing (1) in (10) as follows:

$$R_{pm,qn}(t_1, t_2; \omega_1, \omega_2)$$
$$= E\Bigg[\sum_{i_1, i_2 = 1}^{I} \Big\{ G_p^B(\Theta_{i_1}^B, \Omega_{i_1}^B; \omega_1) G_m^M(\Theta_{i_1}^M, \Omega_{i_1}^M; \omega_1) g_{p,m;i_1}$$
$$\times e^{-j\omega_1 \tau_{p,m;i_1}(t_1)} e^{j(\phi_{i_1} - \phi_{i_2})} e^{j\omega_2 \tau_{q,n;i_2}(t_2)}$$
$$\times G_q^{B*}(\Theta_{i_2}^B, \Omega_{i_2}^B; \omega_2) G_n^{M*}(\Theta_{i_2}^M, \Omega_{i_2}^M; \omega_2) g_{q,n;i_2} \Big\} \Bigg]. \quad (11)$$

We decompose the expression of $R_{pm,qn}(t_1, t_2; \omega_1, \omega_2)$ by regrouping dependent and independent variables in (11), replacing g_i from (9) and using Assumptions A6 and A7:

$$R_{pm,qn}(t_1, t_2; \omega_1, \omega_2)$$
$$= \frac{P}{I} \sum_{i_1, i_2 = 1}^{I} \Big\{ E\Big[(\tau_{i_1} \tau_{i_2})^{-\eta/2} e^{j(\omega_2 \tau_{i_2} - \omega_1 \tau_{i_1})} \Big] E\big[e^{j(\phi_{i_1} - \phi_{i_2})} \big]$$
$$\times E\big[G_p^B(\Theta_{i_1}^B, \Omega_{i_1}^B; \omega_1) G_q^{B*}(\Theta_{i_2}^B, \Omega_{i_2}^B; \omega_2)$$
$$\times e^{(j/c)(\omega_1 \mathbf{a}_p^{B^T} \Psi_{i_1}^B - \omega_2 \mathbf{a}_q^{B^T} \Psi_{i_2}^B)} \big]$$
$$\times E\big[G_m^M(\Theta_{i_1}^M, \Omega_{i_1}^M; \omega_1) G_n^{M*}(\Theta_{i_2}^M, \Omega_{i_2}^M; \omega_2)$$
$$\times e^{(j/c)(\omega_1 (\mathbf{a}_m^M - \mathbf{v}t_1)^T \Psi_{i_1}^M - \omega_2 (\mathbf{a}_n^M - \mathbf{v}t_2)^T \Psi_{i_2}^M)} \big] \Big\}. \quad (12)$$

We assume that Ψ_i^M and Ψ_i^B are independent in order to derive the above expression. This assumption is a sufficient (not a necessary) condition which allows to separate the last two expectations. In microcell urban environments, this assumption is accurately valid. However, the proposed model may be fit to approximately characterize some other wireless scattering media. In [17, Appendix I], the following expression is derived for the first expectation of (12):

$$E\big[(\tau_{i_1} \tau_{i_2})^{-\eta/2} \exp(j(\omega_2 \tau_{i_2} - \omega_1 \tau_{i_1})) \big]$$
$$= \begin{cases} \Phi_\tau^{(\eta/2)}(j\omega_2) \Phi_\tau^{(\eta/2)}(-j\omega_1), & i_1 \neq i_2, \\ \Phi_\tau^{(\eta)}(j(\omega_2 - \omega_1)), & i_1 = i_2, \end{cases} \quad (13)$$

where $\Phi_\tau(s) = e^{(\mu-\sigma)s}/(1 - \sigma s)$ is the MGF of the time-delay τ_i and $\Phi_\tau^{(\eta)}(s) = E[\tau^{-\eta} \exp(\tau s)]$ is the η-order integration of the MGF of the delay profile (DP). (If $\eta/2$ is not a positive integer number, fractional integration or numerical methods are required to evaluate $\Phi_\tau^{(\eta/2)}(s)$ [18].) We also have

$$E[e^{j(\phi_{i_1} - \phi_{i_2})}] = \begin{cases} 0, & i_1 \neq i_2, \\ 1, & i_1 = i_2. \end{cases} \quad (14)$$

The last two expectations in (12) are calculated in Appendix A. The calculation is proposed for the case when $i_1 = i_2$ since the corresponding term to $i_1 \neq i_2$ vanishes (because of the fact that $E[e^{j(\phi_{i_1} - \phi_{i_2})}] = 0$ for $i_1 \neq i_2$). Hereby, we formulate the CCF as follows:

$$R_{pm,qn}(t_1, t_2; \omega_1, \omega_2)$$
$$= P \Phi_\tau^{(\eta)}(j(\omega_2 - \omega_1))$$
$$\times \mathcal{W}\big(\mathbf{d}_{p,q}^B, \mathcal{G}_{p;k_1,k_2}^B(\omega_1) \otimes \mathcal{G}_{q;k_1,k_2}^{B*}(\omega_2) \otimes (\mathcal{F}_{A;k_1}^B \mathcal{F}_{E;k_2}^B) \big)$$
$$\times \mathcal{W}\big(\mathbf{d}_{m,n}^M, \mathcal{G}_{m;k_1,k_2}^M(\omega_1) \otimes \mathcal{G}_{n;k_1,k_2}^{M*}(\omega_2) \otimes (\mathcal{F}_{A;k_1}^M \mathcal{F}_{E;k_2}^M) \big), \quad (15a)$$

where,

$$\mathcal{W}(\mathbf{d}, \mathcal{H}_{k_1,k_2})$$
$$\triangleq 2\pi \sum_{k_1, k_2 = -\infty}^{+\infty} \Big\{ \mathcal{H}_{k_1,k_2} j^{k_1} e^{jk_1 \arctan(y/x)}$$
$$\times \int_{-\pi/2}^{\pi/2} e^{j(k_2 \Omega + (z/c)\sin\Omega)}$$
$$\times J_{k_1}\left(\frac{\cos\Omega \sqrt{x^2 + y^2}}{c} \right) d\Omega \Big\}, \quad (15b)$$

$$\mathbf{d}_{p,q}^B \triangleq \omega_1 \mathbf{a}_p^B - \omega_2 \mathbf{a}_q^B,$$
$$\mathbf{d}_{m,n}^M \triangleq (\omega_2 t_2 - \omega_1 t_1) \mathbf{v} + (\omega_1 \mathbf{a}_m^M - \omega_2 \mathbf{a}_n^M), \quad (15c)$$

where $\mathbf{d} \triangleq [x, y, z]^T$ is a separation vector, $\mathcal{G}_{(k_1,k_2)}(\omega)$, $\mathcal{F}_{A;k}$ and $\mathcal{F}_{E;k}$ are the kth FSCs of the APP, the AAS, and the EAS in the corresponding coordinate and/or the corresponding antenna element, respectively, $J_k(u) \triangleq (j^{-k}/\pi) \int_0^\pi e^{j(k\xi + u\cos\xi)} d\xi$ is the kth-order Bessel function of the first kind, and $\otimes$ denotes the 2D linear convolution. The two-dimensional linear convolution of discrete-time signals $x_{m,n}$ and $y_{m,n}$ is denoted and defined by $x_{m,n} \otimes y_{m,n} \triangleq \sum_{k=-\infty}^{+\infty} \sum_{l=-\infty}^{+\infty} x_{k,l} y_{m-k,n-l}$. The separation vectors $\mathbf{d}_{(\cdot)}^{(\cdot)}$ demonstrate the impact of the location of the antenna elements, the time indices, the carrier frequencies, and the MS direction and speed.

Remark 1. For an omnidirectional antenna, we have $\mathcal{G}_{k_1,k_2} = 0$ for $k_1, k_2 \neq 0$. In this case, the corresponding coefficients $\mathcal{G}_{k_1,k_2}$ vanish from the CCF. Similarly, for an isotropic scattering on the azimuth axis around either the BS or the MS, we have $\mathcal{F}_{A;0} = 1/2\pi$ and $\mathcal{F}_{A;k} = 0$ for $k \neq 0$, and we have $\mathcal{F}_{E;k} = 1/2\pi$ for all k. It implies that the corresponding coefficients, $\mathcal{F}_{A;k}$ and $\mathcal{F}_{E;k}$, vanish from the

CCF. In contrast to the isotropic scattering environment [17], the nonisotropic scattering and the propagation patterns together create higher order Bessel functions in the CCF. Since the AASs, the EASs (the pdfs of azimuth and the elevation propagation directions), and the APPs are accurately approximated by a limited number of FSCs, in practice we obtain an accurate approximation for the CCF by employing a limited number of Bessel functions in (15a).

Remark 2. Interestingly, the FSCs of the AAS and the EAS are shown in a multiplicative form. Although we assume that the pdfs of the propagation directions in azimuth and elevation are independent from each other, it is evident that their interaction appears in the final form of the CCF. For the scenario when propagation happens in the 2D azimuth plane, we have $\mathcal{F}_{E;k} = 1/2\pi$ for all k, and $\mathcal{G}_{k_1,k_2} = 0$ for $k_2 \neq 0$, and $\mathcal{G}_{k_1,k_2} = \mathcal{G}_{k_1}$ for $k_2 = 0$. Therefore, the expression of $\mathcal{W}$ is presented by a single summation on a linear combination of Bessel functions of the first kind with different orders.

Remark 3. In general, the calculation of $\mathcal{W}$ in (15b) does not give a closed-form expression. In order to be able to discuss the physical interpretations of the derived mathematical equations, here we propose closed-form solutions when the employed antennas are omnidirectional; that is, $\mathcal{G}_{k_1,k_2} = 0$ for $k_1, k_2 \neq 0$. These closed-form expressions are addressed using different cases introduced for the EAS in (5a) and (5b).

EAS I, $\alpha = 0, z = 0$

This scenario introduces a uniform 3D rich scattering environment, and employing antennas in the 2D azimuth plane. Using Bessel integration on (15a), we get

$$\mathcal{W} = \sum_{k=0}^{\infty} J_l^2 \left(\frac{|\mathbf{d}|}{2c} \right), \quad k = 2l, \ l \in \mathbb{N} \cup \{0\}, \qquad (16)$$

where $|\cdot|$ denotes the Euclidian norm (see [15, page 485] for $\int_0^{\pi/2} J_{2n}(2u \sin(\xi)) d\xi = (\pi/2) J_n^2(u)$). This result is similar to the 2D scenario; investigated in [18]; however, the 3D case introduces powers of the Bessel function [5]. This model is a direct 3D extension of the Clarke/Jake's model [11].

The following closed-form results are obtained for uniform scattering in azimuth, that is, when azimuths of DODs and DOAs are independently and uniformly distributed over $[0, 2\pi)$.

EAS I, $\alpha = 1/2, z = 0$

This scenario introduces uniformly distributed scatterers on a sphere. Using the Bessel integration expression (see [15, page 485] for $\int_0^{\pi/2} J_\zeta(u \sin(\xi)) \sin^{\zeta+1}(\xi) \cos^{2\nu+1}(\xi) d\xi = (2^\nu \Gamma(\nu + 1)/u^{\nu+1}) J_{\zeta+\nu+1}(u)$, $\text{Re}(\zeta) > -1$, $\text{Re}(\nu) > -1$.) and $J_{1/2}(u) = \sqrt{2/\pi}(\sin(u)/\sqrt{u})$ [15, page 437], we get

$$\mathcal{W} = \frac{\sin\left(\sqrt{x^2 + y^2}/c\right)}{\sqrt{x^2 + y^2}/c} \triangleq \text{sinc}\left(\frac{\sqrt{x^2 + y^2}}{c} \right). \qquad (17)$$

This result is consistent with some available results in the literature [5].

EAS I, $x = y = 0$

This scenario studies the vertical separation of antenna elements in a microcellular propagation environment. Antenna elements are located at the origin of the azimuth plane. Using the Bessel integration (see [15, page 360] for $J_\nu(u) = (((1/2)u)^\nu/\sqrt{\pi}\Gamma(\nu + 1/2)) \int_0^\pi \cos(u \cos(\xi)) \sin^{2\nu}(\xi) d\xi$), we get

$$\mathcal{W} = \frac{\Gamma(\alpha + 1)}{(z/2c)^\alpha} J_\alpha \left(\frac{z}{c} \right). \qquad (18)$$

Using the proposed results in this scenario, we are able to study different 3D propagation environments by changing the degree of urbanization, α.

EAS II; $z = 0$

Using (5b) and the Bessel integration [15, page 485], we get

$$\mathcal{W} = \frac{(2c)^{\alpha+3/2} \Gamma(\alpha + 1/2)}{c(2\alpha + 1)(x^2 + y^2)^{\alpha/2+1/4}} J_{\alpha+1/2} \left(\frac{\sqrt{x^2 + y^2}}{c} \right). \qquad (19)$$

This simple expression is an extension of the Clarks model for isotropic propagation.

Remark 4. From (15b) we observe that the expression $\arctan(y/x)$ modulates the coefficients of the linear combination of averaged Bessel functions, that is, $e^{jk_1 \arctan(y/x)} \mathcal{H}_{k_1,k_2}(\omega_1, \omega_2)$. This phase modulation significantly affects the behavior of the CCF. This phase is a function of the direction of the MS speed, that is, $\angle \mathbf{v}$. Therefore, the direction of the MS speed plays an important role in the behavior of the CCF. Obviously in an isotropic environment and using omnidirectional antennas, this phase modulation vanishes. More investigation on this problem is addressed in the next section.

Remark 5. The components $\Phi_\tau^{(\eta/2)}(-j\omega_1)\Phi_\tau^{(\eta/2)}(j\omega_2)$ and $\Phi_\tau^{(\eta)}(j(\omega_2 - \omega_1))$ describe the impact of the delay profile (exponential profile) and the pathloss exponent on the cross-correlation between CTFs. The CCF also depends on the carrier frequencies, ω_1, ω_2 via $\mathbf{d}^B$ and $\mathbf{d}^M$.

Remark 6. The proposed 3D model takes into account the antenna heights. The vertical separation of antenna elements is the result of their different heights. Such a difference in the antenna heights produces phase differences between the received or the transmitted signals, and consequently puts impacts on the CCF. This property can be employed to improve the space diversity in MIMO wireless systems.

4. NUMERICAL EVALUATION OF THE 3D CROSS-CORRELATION FUNCTION (CCF)

In this section, the CCF is numerically analyzed under different circumstances. This analysis consists of frequency-domain analysis and time-domain analysis. Such an analysis illustrates that the nonuniform distribution of scatterers in the 3D space along with the 3D directional APPs has major impact on the 3D-CCF.

4.1. Analysis of the 3D-CCF in stationary scenario

In order to see the temporal variations of the wireless channel in a 3D propagation medium on the MS side, we analyze the CCF in the frequency domain. This analysis is performed on a simple stationary scenario for a multiple-input single-output (MISO) wireless channel on the MS side when $\omega_1 = \omega_2 \triangleq \omega$, $\kappa^2 = 0$, and $m = n = 1$. In this case from $\angle \mathbf{d}_{1,1}^M = \angle \mathbf{v} + \angle(t_1 - t_2)$ and $R_{1p,1q}(t_1, t_2; \omega, \omega) = R_{1p,1q}(\Delta t; \omega)$, we get

$$
\begin{aligned}
&R_{1p,1q}(\Delta t; \omega) \\
&= 2\pi P \mathcal{W}\left(\mathbf{d}_{p,q}^B, \mathcal{G}_{p;k_1,k_2}^B(\omega) \otimes \mathcal{G}_{q;k_1,k_2}^B{}^*(\omega) \otimes (\mathcal{F}_{A;k_1}^B \mathcal{F}_{E;k_2}^B)\right) \\
&\quad \times \sum_{k_1,k_2=-\infty}^{+\infty} \left\{ \left(\mathcal{G}_{1;k_1,k_2}^M(\omega) \otimes \mathcal{G}_{1;k_1,k_2}^M{}^*(\omega) \otimes (\mathcal{F}_{A;k_1}^M \mathcal{F}_{E;k_2}^M)\right) \right. \\
&\quad \left. \times j^{k_1} e^{jk_1 \angle \mathbf{v}} \int_{-\pi/2}^{\pi/2} e^{jk_2\Omega} J_{k_1}\left(\cos\Omega \frac{\omega |\mathbf{v}|}{c} \Delta t\right) d\Omega \right\},
\end{aligned}
\tag{20}
$$

where $\Delta t \triangleq t_2 - t_1$ is the time-difference index. Using (20) and the Fourier transform of $J_k(u)$, the Fourier transform of this CCF versus Δt results in $(R_{1p,1q}(\Delta t; \omega) \leftrightarrow \mathbf{R}_{1p,1q}(\Lambda, \omega))$:

$$
\begin{aligned}
&\mathbf{R}_{1p,1q}(\Lambda, \omega) \\
&\triangleq \int_{-\infty}^{+\infty} e^{-j\Lambda\Delta t} R_{1p,1q}(t_1, t_2; \omega, \omega) d\Delta t \\
&= \frac{4\pi c}{\omega |\mathbf{v}|} P \mathcal{W}_{p,q}^B \\
&\quad \times \sum_{k_1,k_2=-\infty}^{+\infty} \left\{ \left(\mathcal{G}_{1;k_1,k_2}^M(\omega) \otimes \mathcal{G}_{1;k_1,k_2}^M(\omega) \otimes (\mathcal{F}_{A;k_1}^M \mathcal{F}_{E;k_2}^M)\right) e^{jk_1 \angle \mathbf{v}} \right. \\
&\quad \left. \times \int_{-\pi/2}^{\pi/2} \frac{e^{jk_2\Omega} T_{k_1}(c\Lambda/|\mathbf{v}|\omega\cos\Omega)}{\cos\Omega\sqrt{1 - (c\Lambda/|\mathbf{v}|\omega\cos\Omega)^2}} d\Omega \right\},
\end{aligned}
\tag{21}
$$

where Λ is the frequency representative of the Doppler shift in the frequency domain and $T_k(\Lambda) \triangleq \cos[k\cos^{-1}(\Lambda)]$ is the Chebyshev polynomial of the first kind. The following, $\mathbf{R}^M(\Lambda)$, represents the impact of the nonisotropic 3D environment, the directional APP, and the speed on the MS side:

$$
\begin{aligned}
&\mathbf{R}^M(\Lambda) \\
&\triangleq \sum_{k_1,k_2=-\infty}^{+\infty} \left\{ \left(\mathcal{G}_{1;k_1,k_2}^M(\omega) \otimes \mathcal{G}_{1;k_1,k_2}^M{}^*(\omega) \otimes (\mathcal{F}_{A;k_1}^M \mathcal{F}_{E;k_2}^M)\right) e^{jk_1 \angle \mathbf{v}} \right. \\
&\quad \left. \times \int_{-\pi/2}^{\pi/2} \frac{e^{jk_2\Omega} T_{k_1}(c\Lambda/|\mathbf{v}|\omega\cos\Omega)}{\cos\Omega\sqrt{1 - (c\Lambda/|\mathbf{v}|\omega\cos\Omega)^2}} d\Omega \right\}.
\end{aligned}
\tag{22}
$$

The term $\mathbf{R}^M(\Lambda)$ is a power spectral density (PSD) that represents the temporal channel variations caused by the MS speed. Because there is no closed-form for this PSD, it may be numerically evaluated in terms of different parameters as combinations of different APPs, AASs, EASs, and direction of MS speed. The major concern of the current analysis is to see the effects of propagation in the third dimension (elevation), therefore we assume a fixed AAS that represents a typical

macrocellular urban environment: the AAS is Laplacian distributed with the parameter $a = 0.25$ rad (the FSCs are given by $\mathcal{F}_{A;k} = (e^{-\pi/a}(-1)^{k+1} + 1)/2\pi(1 - e^{-\pi/a})(1 + k^2 a^2)$. In Figures 4 and 5, this PSD is depicted for several scenarios that are produced by combinations of the following:

(1) distribution of propagation directions on the third dimension around the MS (EAS distribution): EAS I or EAS II distributions with different values of α;

(2) antenna propagation pattern: half-wavelength dipole or horizontal wavelength dipole with the size of $h = c/2f$;

(3) direction of the MS speed: the positive x-axis direction in Figure 4 or the positive y-axis direction in Figure 5.

The figures show that the maximum Doppler shift is $\omega|\mathbf{v}|/c$ (i.e., $\mathbf{R}^M(\Lambda) = 0$, if $|\Lambda| \geq \omega|\mathbf{v}|/c$). In the 3D propagation environment, the direction of the MS speed has a less significant impact on the behavior of the CCF comparing with the 2D nonisotropic propagation scenario which is studied in [18]. In other words, the 3D-CCF appears as an averaged form of the 2D-CCF when the averaging is being applied on the elevation angle. Therefore, due to this averaging, the FSCs of the EAS pdf have a more dominant effect on the CCF. In a 2D propagation environment, the direction of the MS speed along with the type of the AAS (waves coming from the azimuthal direction) substantially affects the CCF. In contrast, in a 3D propagation environment, the CCF is influenced by the dominant waves coming from both azimuthal and elevation directions. Since the number of incoming waves from the elevation direction are almost invariant with the speed of MS, the MS speed has a reduced impact on the CCF in a 3D environment compared to a 2D scattering environment [18]. In contrast to the 2D propagation, for example, in the Clarks model [11], the tails of the PSD graphs in the 3D scenario do not go to infinity, that is, the U-shaped graphs of the PSD in the 2D scenario are modified into the flat V-shaped PSD graphs in the 3D scenario. This result is consistent with the result proposed by Parsons and Turkmani [19]. We also note that the shape of the spectrum around $\Lambda = 0$ is deviated from being flat. This deviation is produced by the directional response of the antennas.

The shape of the derived PSD is not very sensitive to the variations of the urbanization factor α, or to the variations of the type of the employed antenna; however, this shape significantly changes when we change EAS I into EAS II. This suggests that the EAS pdfs in (5a) and (5b) represent two distinct wave propagation mechanisms. Therefore, a realistic linear convex combination of this family could realistically fit a nonisotropic environment in the third dimension.

4.2. Coherence bandwidth, coherence time, and spatial correlation

We evaluate the coherence time (CT) and the coherence bandwidth (CB) in terms of different related parameters. The CT, T_c, is the separation time over which the fading
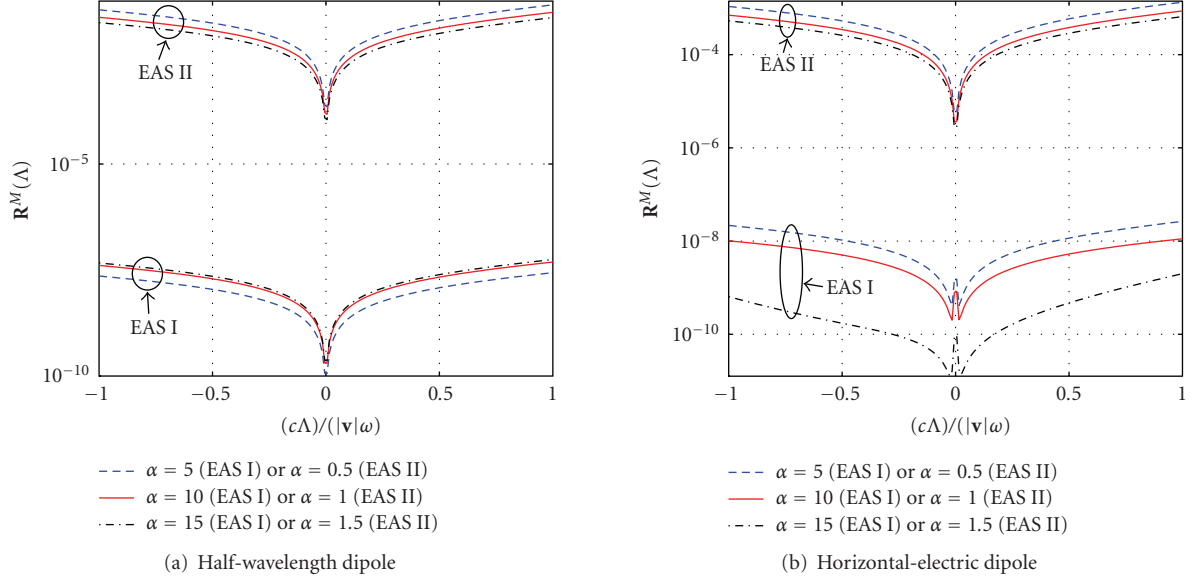
FIGURE 4: *Power spectral density (PSD) for 3D propagation, when MS moves on the positive direction of the x-axis*, for stationary CCF ($\omega_1 = \omega_2 = \omega$, $\kappa^2 = 0$, and $m = n = 1$), $|\mathbf{v}| = 50$ Km/h, for two nonisotropic EAS pdfs (EAS I and EAS II pdfs), and nonisotropic AAS (Laplacian pdf with $a = 0.25$): (a) half-wavelength dipole and (b) horizontal-electric dipole.

channel remains almost unchanged, and the CB, B_c, is the separation between frequencies over which the channel gain is almost constant. A conventional definition for these coherence functions in a single-input single-output (SISO) communication system is the value of Δ ($\Delta t = t_2 - t_1 \geq 0$ or $\Delta\omega = \omega_2 - \omega_1 \geq 0$) which satisfies the equation of the envelope correlation $\rho_{\Delta t,0} = 0.5$ or $\rho_{0,\Delta\omega} = 0.5$, where $\rho_{\Delta t,\Delta\omega} \triangleq (E[r(t_1;\omega_1)r(t_2;\omega_2)] - E^2[r(t,\omega)])/(E[r^2(t;\omega)] - E^2[r(t,\omega)])$, $r(t,\omega) \triangleq |h(t,\omega)|$ and $E[r(t,\omega)] = (1/2)\sqrt{\pi R(t,t;\omega,\omega)}$ [11, 30]. This definition is equivalent to $D_{\Delta t,\Delta\omega} \triangleq |R(t_1,t_2;\omega_1,\omega_2)|^2/|R(t_i,t_i;\omega_i,\omega_i)|^2 = 0.5$ (see Appendix B). Therefore, using the expression of the CCF in (15a), the CB and the CT are given by solving $D_{0,\Delta\omega} = 0.5$ and $D_{\Delta t,0} = 0.5$ for $\Delta\omega$ and Δt, respectively.

4.2.1. Coherence bandwidth

The CB is a characteristic of the random propagation environment and may be independently investigated from the employed antenna array. This is justified by the Kronecker product form of the CCF and because the response of the employed antenna array (in terms of the carrier frequency) could be taken into account, separately. The CB characterizes the behavior of multicarrier propagation for a SISO communication system. The CB is defined as the solution of $D_{0,\Delta\omega} = 0.5$ for $\Delta\omega$. Our numerical evaluations derived from this model show that, in practical situations, the CB mostly depends on the delay spread σ ($t_1 = t_2 = 1$ second), that is, it is almost invariant with variations of the parameters of the nonisotropic propagation medium, the employed antennas, or the MS speed. In other words,

the CB for an outdoor propagation environment is mostly determined by the delay spread of the DP, σ.

Consistent with the behavior of wide-sense-stationary uncorrelated-scattering (WSSUS) systems [31], the proposed CCF in a stationary scenario suggests a WSSUS propagation system for outdoor environments. Figure 6 shows the CB with respect to σ for a typical urban environment ($\eta = 2$), for crowded urban environment ($\eta = 4$) and for rural environment ($\eta = 6$). These values for the CB are close to the average of reported experimental measurements in the literature [28, 32–34]. The reported values in the literature are between 11.5 MHz to 1.2 MHz [33] for delay spread values of 0.1 microseconds to 2 microseconds [32] in outdoor propagation environments. It turns out that, the CB values reported in the literature under various conditions are accurately predicted using the proposed model. For example, when $|R| = 0.5$, Rappaport in [35] reported an approximation formula for the CB as CB $\approx 1/5\sigma$. This formula results in CB = 0.2 MHz for $\sigma = 1$ microseconds which is very close to what is predicted by (23). In order to suggest more accurate formulas for the CB in outdoor environments, Figure 6 illustrates an almost linear relation between the CB and the time delay spread σ in a log-log scale, that is, using a simple curve fitting, we have

$$\text{CB} \approx k_1\sigma^{k_2}, \begin{cases} k_1 = 8.9450, & k_2 = -0.7432; & \eta = 2, \\ k_1 = 81.4346, & k_2 = -0.6088; & \eta = 4, \\ k_1 = 351.6372, & k_2 = -0.5212; & \eta = 6. \end{cases}$$
$$(23)$$

The error in this approximation is less than ± 0.75 dB in $|R|$, when the delay spread lies in [0.1–1.1] microseconds (the reported range of delay spread for outdoor environments).
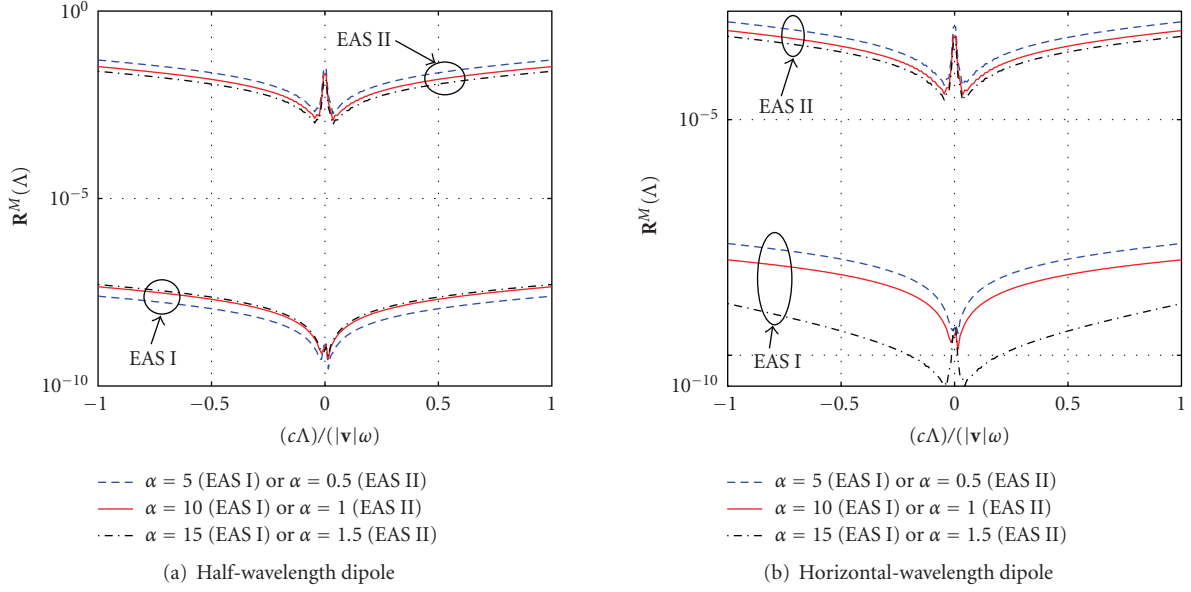
FIGURE 5: *Power spectral density (PSD) for 3D propagation when MS moves on the positive direction of the y-axis*, for stationary CCF ($\omega_1 = \omega_2 = \omega$, $\kappa^2 = 0$, and $m = n = 1$), $|\mathbf{v}| = 50$ Km/h, for two nonisotropic EAS pdfs (EAS I and EAS II pdfs), and nonisotropic AAS (Laplacian pdf with $a = 0.25$). (a) Half-wavelength dipole, (b) horizontal-electric dipole.
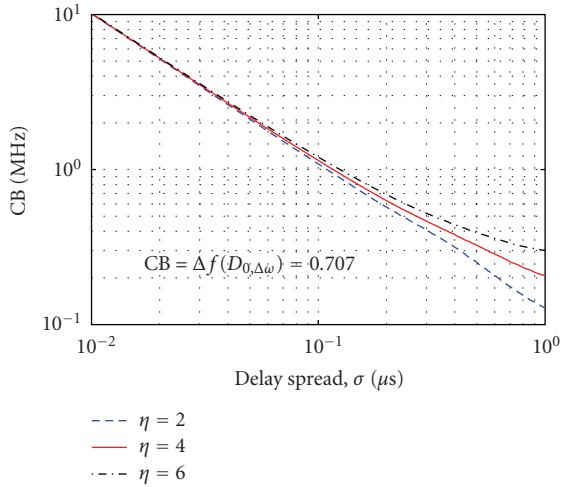

FIGURE 6: *Coherence bandwidth*, with respect to the delay spread σ; using exponential DP with mean, $\overline{\tau} = 3.33$ microseconds, $t_1 = t_2 = 1$ second, $f_1 = 4$ GHz, $\kappa^2 = 0$, SISO communication system and for different propagation environments with different pathloss exponents η: free space (typical urban), crowded urban or rural environments with $\eta = 2, 4$, or 6, respectively.

4.2.2. Coherence time

Our numerical investigations show that the CT is a function of the value of the MS speed (or the maximum Doppler shift), and other parameters such as the EAS pdf. This result is expected based on the Fourier analysis on the stationary CCF, as the Doppler effect certainly appears as a function of different parameters of the nonisotropic propagation medium and parameters of the employed antenna. As the

results of the Fourier analysis of the CCF do not significantly depend on the direction of the MS or the value of α, the CT is only evaluated in two different cases of EASs with fixed αs and employing two different antennas. The CT is defined as $\Delta t (D_{\Delta t,0} = 0.5)$. Figure 7 shows the CT with respect to the value of the MS speed in a log-log scale. All these graphs exhibit an almost linear relation between the value of the MS speed and the CT in a log-log scale, particularly when we use horizontal-electric antenna. We point out that the average CT with EAS I is larger compared to the EAS II. The CT average value results are in consistency with available approximation formulas for the CT in the literature. For example, when $|R| = 0.5$, Rappaport in [35] reports an approximation formula for the CT as CT $\approx 9c/8|\mathbf{v}|\omega$, where c is the speed of light and ω is the carrier frequency. Given $|\mathbf{v}| = 60$ Km/h and $\omega = 2\pi f$ with $f = 1$ GHz, this formula results in CT $= 32.22$ milliseconds which is very close to the results of our model in the scenario of EAS I. In order to suggest more accurate formulas for the CT in outdoor environments, we use the same curve-fitting technique being employed for the CB. This way, we find a simple linear approximation between the CT and $|\mathbf{v}|$ as follows (horizontal-electric antenna):

$$\text{CT} \approx k_1 |\mathbf{v}|^{k_2}, \quad \begin{cases} k_1 = 11.2934, & k_2 = -1.2112; \\ & \text{EAS I; } \alpha = 10, \\ k_1 = 8.5378, & k_2 = -1.2103; \\ & \text{EAS II; } \alpha = 1. \end{cases} \quad (24)$$

4.2.3. Spatial correlation

We evaluate the effect of multiple directional antennas and their spatial separations at the transmitter/receiver sides
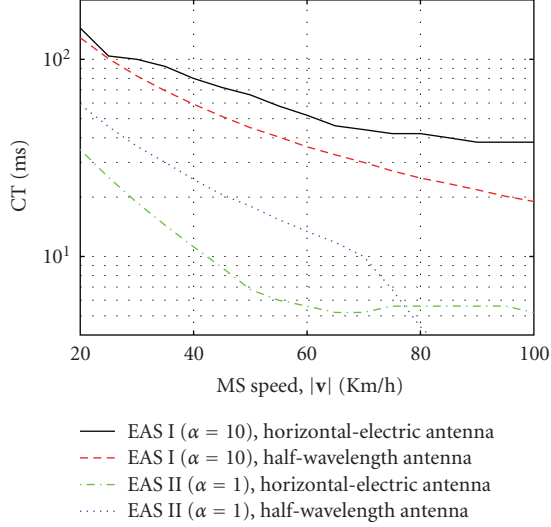
FIGURE 7: *Coherence time*, with respect to the value of the MS speed $|\mathbf{v}|$, considering two different EASs: EAS I ($\alpha = 10$) and EAS II ($\alpha = 1$), Laplacian AAS pdf ($a = 0.25$ rad), using exponential DP with $\bar{\tau} = 3.33$ microseconds, $\sigma = 1$ microseconds, $f_1 = f_2 = 1$ GHz, and for a SISO communication system; employing half-wavelength antenna or horizontal-electric antenna.

on the CCF by the spatial coherence (SC) and the spatial correlation coefficient (SCC). In order to evaluate the SC at the transmitter (or the receiver) and analogous to the definition of the CT and the CB, we define the SC with respect to the antenna separation on the x-axis of the azimuthal plane as the solution of $\Delta x = |R_{p1,q1}/R_{11,11}| = 0.5$. It is noted that the SC could be defined for any direction or as a nonnegative matrix where results turn out to be similar. Our simulation results show that the SCC at the transmitter, that is, $|R_{p1,q1}/R_{11,11}|$ (or at the receiver, i.e., $|R_{1m,1n}/R_{11,11}|$) decreases when the distance between two antennas on the azimuthal plane increases. These variations depend on the response of the APP main-lobes of two directional antennas and the type of propagation on the azimuth and the elevation, that is, the SC is a function of the parameters of the AAS and the EAS pdfs, the antenna array response, and the relative position of antennas with respect to each other. Figure 8 shows the SC or Δx as a function of multicarrier frequency separations for a MIMO communication system employing different antenna types and using Laplacian AAS and EAS I. We observe that this SC curve is almost linear in the log-log scale. Using the same curve-fitting technique, we suggest the following approximations between Δx measured in wavelength $\lambda_1 = c/f_1$ and Δf measured in GHZ (for Laplacian AAS and EAS I with $\alpha = 10$):

$$SC_x \triangleq \Delta x \approx k_1 (\Delta f)^{k_2},$$

$$\text{where} \begin{cases} k_1 = 0.9585, & k_2 = -0.2526; \\ & \text{using Half-wavelength dipole,} \\ k_1 = 1.0496, & k_2 = -0.2526; \\ & \text{using Horizontal-electric dipole.} \end{cases}$$
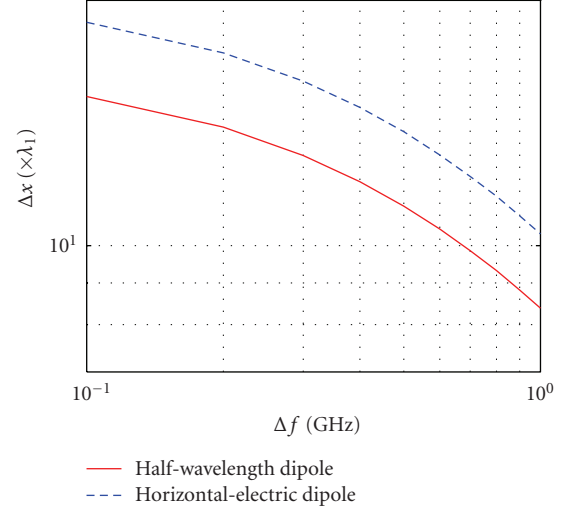
$$(25)$$

FIGURE 8: *Spatial coherence*, with respect to separation between two multicarrier frequencies Δf, considering EAS I ($\alpha = 10$), Laplacian AAS pdf ($a = 0.25$ rad), using exponential DP with $\bar{\tau} = 3.33$ microseconds, $\sigma = 2$ microseconds, $f_1 = 1$ GHz, $f_2 = f_1 + \Delta f$, and for a MIMO communication system at the transmitter station (BS) when one antenna is located at the center of the azimuthal plane and the other is located on the x-axis with the separation distance Δx; employing half-wavelength dipole or horizontal-electric dipole with the length of $h = c/2f$.

The proposed CCF takes also into account the effect of antenna elements which are located outside the horizontal plane. Figure 9 shows the SCC at the transmitter, $|R_{p1,q1}/R_{11,11}|$, for a scenario where two antennas are vertically separated from each other on the z-axis. Using half-wavelength dipole and horizontal-electric dipole, and assuming EAS I and EAS II for the elevation propagation, from our evaluations we observe that the decaying slope of the CCF mostly depends on the type of propagation in elevation, EAS I or EAS II. Evidently, such an SCC curve depends also on the carrier frequencies.

5. CONCLUSIONS

We have calculated the CCF for a MIMO multicarrier channel in a 3D outdoor environment. The novelty of this 3D-CCF is that it considers the impact of nonisotropic wave propagation along with directional antenna propagation patterns. Our derivation is a nongeometry approach as in [17] where the nonisotropic environment and the antenna pasterns are described by their Fourier series expansions. The proposed CCF turns out to be the multiplication of three correlation functions. The first function is characterized by the parameters of the antennas at the BS and the scatterers around the BS. Similarly, the second function is characterized by the parameters of the antennas at the MS and the scatterers around the MS. The last one describes the impact of the delay profile and the pathloss component (see [17] for more details about this term). The first two CCFs (in each station) appear as a linear series expansion of averaged Bessel
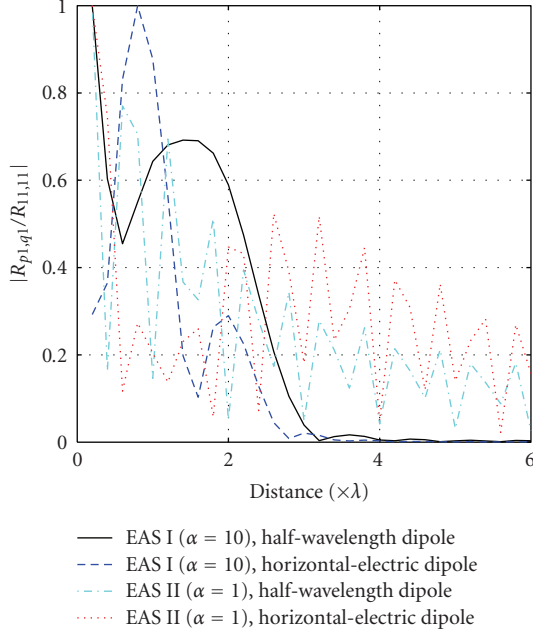
FIGURE 9: *Spatial correlation coefficient*, with respect to vertical distance in wavelength λ between two directional antennas located at the center of the azimuthal plane (one is located at $z = 0$), considering two different EASs: EAS I ($\alpha = 10$) and EAS II ($\alpha = 1$), Laplacian AAS pdf ($a = 0.25$ rad), using exponential DP with $\overline{\tau} = 3.33$ microseconds, $\sigma = 2$ microseconds, $f_1 = f_2 = 1$ GHz, and for a MIMO communication system at the transmitter station (BS); employing half-wavelength dipole or horizontal-electric dipole.

functions of the first kind. The coefficients of this expansion are given by the 2D linear convolution of the FSCs of the corresponding antenna propagation patterns with the FSCs of the nonisotropic distributions of the angles of scatterers. In practice, this expansion has a limited number of components since the coefficients converge to zero rapidly. Our numerical evaluations on the CCF revealed that the power spectrum density is sensitive to the environment type (i.e., to the shape of the pdf of the EAS) and the characteristics of the employed antenna on the MS side. We also proposed formulas for approximation of the coherence bandwidth, the coherence time, and the spatial coherence using the proposed CCF. These approximations are accurately close to the corresponding empirical results reported in the literature for realistic outdoor propagation channels. The SC is impacted by the effect of the antenna separation, the APPs, the multicarrier frequency separation, and the propagation environment.

APPENDICES

A. CALCULATION OF THE CROSS-CORRELATION FUNCTION

This appendix provides details of the calculation of the last two expectations in (12), that is,

$$E\left[G_p^B(\Theta_{i_1}^B, \Omega_{i_1}^B; \omega_1) G_q^{B*}(\Theta_{i_2}^B, \Omega_{i_2}^B; \omega_2) e^{(j/c)(\omega_1 \mathbf{a}_p^{B^T}\Psi_{i_1}^B - \omega_2 \mathbf{a}_q^{B^T}\Psi_{i_2}^B)}\right],$$

$$E\left[G_m^M(\Theta_{i_1}^M, \Omega_{i_1}^M; \omega_1) G_n^{M*}(\Theta_{i_2}^M, \Omega_{i_2}^M; \omega_2)\right.$$
$$\left.\times e^{(j/c)(\omega_1(\mathbf{a}_m^M - \mathbf{v}t_1)^T \Psi_{i_1}^B - \omega_2(\mathbf{a}_n^M - \mathbf{v}t_2)^T \Psi_{i_2}^B)}\right]$$

(A.1)

in which $\Psi_i \triangleq [\cos(\Omega_i)\cos(\Theta_i), \cos(\Omega_i)\sin(\Theta_i), \sin(\Omega_i)]^T$ [15] (see Figure 1 and the list of notations in Section 2). The calculation is proposed for the case when $i_1 = i_2$ since $E[e^{j(\phi_{i_1} - \phi_{i_2})}] = 0$ for $i_1 \neq i_2$.

Using the FSEs for APPs, AASs, and EASs, we calculate the expectations either at the BS or at the MS. As an example, we evaluate this expression at the MS with antennas m and n. In this situation, we have

$$E\left[G_m^M(\Theta_i^M, \Omega_i^M; \omega) G_n^{M*}(\Theta_i^M, \Omega_i^M; \omega_2) e^{(j/c)\mathbf{d}_{m,n}^{M^T}\Psi_i^M}\right]$$

$$E\left[\left(\sum_{k_1^m, k_2^m} \mathcal{G}_{m;k_1^m, k_2^m}^M(\omega_1) e^{k_1^m \Theta_i^M} e^{k_2^m \Omega_i^M}\right)\right.$$
$$\left.\times \left(\sum_{k_1^n, k_2^n} \mathcal{G}_{n;k_1^n, k_2^n}^{M*}(\omega_2) e^{-k_1^n \Theta_i^M} e^{-k_2^n \Omega_i^M}\right) e^{(j/c)\mathbf{d}_{m,n}^{M^T}\Psi_i^M}\right],$$

(A.2)

where $\mathbf{d}_{m,n}^M \triangleq (\omega_2 t_2 - \omega_1 t_1)\mathbf{v} + (\omega_1 \mathbf{a}_m^M - \omega_2 \mathbf{a}_n^M)$ and $\mathcal{G}_{m;k_1^m, k_2^m}^M(\omega_1)$ and $\mathcal{G}_{n;k_1^n, k_2^n}^M(\omega_2)$ are the FSCs of the APPs. Using the definitions for Ψ_i^M and $\mathbf{d}_{m,n}^M$, we get

$$\exp\left\{\frac{j}{c}\mathbf{d}_{m,n}^{M^T}\Psi_i^M\right\}$$
$$= e^{(j/c)\sin(\Omega_i^M)z_{m,n}^M}$$
$$\times e^{(j/c)[\cos\Omega_i^M \sqrt{x_{m,n}^{M^2} + y_{m,n}^{M^2}}\sin(\Theta_i^M - \arctan(x_{m,n}^M/y_{m,n}^M))]}.$$

(A.3)

Then, we substitute (A.3) in the integral form of (A.2), where the distributions of AAS and EAS are represented by $f_A^M(\Theta_i^M) = \sum_{k=-\infty}^{+\infty} \mathcal{F}_{A;k}^M e^{jk\Theta_i^M}$ and $f_E^M(\Omega_i^M) = \sum_{k=-\infty}^{+\infty} \mathcal{F}_{E;k}^M e^{jk\Omega_i^M}$, respectively. After doing some manipulations, we get

$$E\left[G_m^M(\Theta_i^M, \Omega_i^M; \omega) G_n^{M*}(\Theta_i^M, \Omega_i^M; \omega_2) e^{(j/c)\mathbf{d}_{m,n}^{M^T}\Psi_i^M}\right]$$

$$= 2\pi \sum_{k_1, k_2 = -\infty}^{+\infty}\left\{(\mathcal{G}_{m;k_1, k_2}^M(\omega_1) \otimes \mathcal{G}_{n;k_1, k_2}^{M*}(\omega_2)\right.$$
$$\otimes (\mathcal{F}_{A;k_1}^M \mathcal{F}_{E;k_2}^M)) j^{k_1} e^{jk_1 \arctan(y_{m,n}^M/x_{m,n}^M)}$$
$$\times \int_{\pi/2}^{\pi/2}\left\{e^{jk_2 \Omega_i^M} e^{j(z_{m,n}^M/c)\sin(\Omega_i^M)} J_{k_1}\right.$$
$$\left.\left.\times \left(\cos(\Omega_i^M)\frac{\sqrt{x_{m,n}^{M^2} + y_{m,n}^{M^2}}}{c}\right)\right\}d\Omega_i^M\right\},$$

(A.4)

where $J_k(u) \triangleq (j^{-k}/\pi)\int_0^\pi e^{ju\cos\xi}\cos(k\xi)d\xi$ is the kth-order Bessel function of the first kind, and $\otimes$ denotes linear convolution. The same calculation procedure is valid for the BS side with $\mathbf{d}_{p,q}^B \triangleq (\omega_1 \mathbf{a}_P^B - \omega_2 \mathbf{a}_q^B)$ and APPs on the BS side.

B. THE RELATIONSHIP BETWEEN CCF AND THE ENVELOPE PROCESS $r(t; \omega)$

For the envelope process $r(t; \omega)$ in the presence of enough number of multipath waves (where I is large enough), and for $i = 1$ or $i = 2$, we have [11, pages 47–51]

$$
\begin{aligned}
&E[r(t_1; \omega_1) r(t_2; \omega_2)] \\
&= \frac{1}{2} |R(t_i, t_i; \omega_i, \omega_i)| \left(1 + \sqrt{D_{\Delta t, \Delta \omega}}\right) \mathcal{E}\left(\frac{2\sqrt[4]{D_{\Delta t, \Delta \omega}}}{1 + \sqrt{D_{\Delta t, \Delta \omega}}}\right),
\end{aligned}
\tag{B.1}
$$

where $\mathcal{E}(\cdot)$ represents the complete Elliptic integral of the second kind [15] and $D_{\Delta t, \Delta \omega} \triangleq |R(t_1, t_2; \omega_1, \omega_2)|^2 / |R(t_i, t_i; \omega_i, \omega_i)|^2$. We approximate this equation using the expansion of the hypergeometric function [11, page 51], and obtain

$$
E[r(t_1; \omega_1) r(t_2; \omega_2)] \approx \frac{\pi}{4} |R(t_i, t_i; \omega_i, \omega_i)| \left(1 + \frac{D_{\Delta t, \Delta \omega}}{4}\right).
\tag{B.2}
$$

From the above, we get $\rho_{\Delta t, \Delta \omega} = D_{\Delta t, \Delta \omega} = 0.5$. Therefore, using the expression of the CCFs in this dissertations, the CB and the CT are given by solving one of the following equations, respectively, for $\Delta \omega$ and Δt:

$$
D_{0, \Delta \omega} = 0.5, \qquad D_{\Delta t, 0} = 0.5.
\tag{B.3}
$$

From (B.3) we observe that the CB and the CT are functions of various parameters such as the APP of the employed antenna at the MS, AAS of the propagation environment on the MS side, and the speed of the MS.

ACKNOWLEDGMENT

REFERENCES

[1] H. Bölcskei, M. Borgmann, and A. J. Paulraj, "Impact of the propagation environment on the performance of space-frequency coded MIMO-OFDM," *IEEE Journal on Selected Areas in Communications*, vol. 21, no. 3, pp. 427–439, 2003.

[2] A. Abdi and M. Kaveh, "A space-time correlation model for multielement antenna systems in mobile fading channels," *IEEE Journal on Selected Areas in Communications*, vol. 20, no. 3, pp. 550–560, 2002.

[3] M. Kalkan and R. H. Clarke, "Prediction of the space-frequency correlation function for base station diversity reception," *IEEE Transactions on Vehicular Technology*, vol. 46, no. 1, pp. 176–184, 1997.

[4] Y. Mohasseb and M. P. Fitz, "A 3D spatio-temporal simulation model for wireless channels," in *Proceedings of the IEEE International Conference on Communications (ICC '01)*, vol. 6, pp. 1711–1717, Helsinki, Finland, June 2001.

[5] T. D. Abhayapala, T. S. Pollock, and R. A. Kennedy, "Characterization of 3D spatial wireless channels," in *Proceedings of the 58th IEEE Vehicular Technology Conference (VTC '03)*, vol. 1, pp. 123–127, Orlando, Fla, USA, October 2003.

[6] S. K. Yong and J. S. Thompson, "A three-dimensional spatial fading correlation model for uniform rectangular arrays," *IEEE Antennas and Wireless Propagation Letters*, vol. 2, no. 1, pp. 182–185, 2003.

[7] Q. Yao and M. Pätzold, "Spatial-temporal characteristics of a half-spheroid model and its corresponding simulation model," in *Proceedings of the 59th IEEE Vehicular Technology Conference (VTC '04)*, vol. 1, pp. 147–151, Milan, Italy, May 2004.

[8] S.-Y. Leong, Y. R. Zheng, and C. Xiao, "Space-time fading correlation functions of a 3-D MIMO channel model," in *Proceedings of IEEE Wireless Communications and Networking Conference (WCNC '04)*, vol. 2, pp. 1127–1132, Atlanta, Ga, USA, March 2004.

[9] M. K. Özdemir, H. Arslan, and E. Arvas, "On the correlation analysis of antennas in adaptive MIMO systems with 3-D multipath scattering," in *Proceedings of IEEE Wireless Communications and Networking Conference (WCNC '04)*, vol. 1, pp. 295–299, Atlanta, Ga, USA, March 2004.

[10] P. D. Teal, T. D. Abhayapala, and R. A. Kennedy, "Spatial correlation in non-isotropic scattering scenarios," in *Proceedings of IEEE International Conference on Acoustics, Speech, and Signal Processing (ICASSP '02)*, vol. 3, pp. 2833–2836, Orlando, Fla, USA, May 2002.

[11] W. C. Jakes, *Microwave Mobile Communications*, John Wiley & Sons, New York, NY, USA, 1974.

[12] U. Martin, "Spatio-temporal radio channel characteristics in urban macrocells," *IEE Proceedings: Radar, Sonar and Navigation*, vol. 145, no. 1, pp. 42–49, 1998.

[13] K. I. Pedersen, P. E. Mogensen, and B. H. Fleury, "A stochastic model of the temporal and azimuthal dispersion seen at the base station in outdoor propagation environments," *IEEE Transactions on Vehicular Technology*, vol. 49, no. 2, pp. 437–447, 2000.

[14] A. Tang and K. Gong, "Study on power azimuth spectrum of wireless channel in microcell environments," in *Proceedings of the 14th IEEE Symposium on Personal, Indoor and Mobile Radio Communications (PIMRC '03)*, vol. 1, pp. 685–687, Beijing, China, September 2003.

[15] M. Abramowitz and I. A. Stegun, *Handbook of Mathematical Functions: with Formulas, Graphs, and Mathematical Tables*, Dover, New York, NY, USA, 1974.

[16] H. Hashemi, "The indoor radio propagation channel," *Proceedings of the IEEE*, vol. 81, no. 7, pp. 943–968, 1993.

[17] S. Gazor and H. S. Rad, "Space-time-frequency characterization of MIMO wireless channels," *IEEE Transactions on Wireless Communications*, vol. 5, no. 9, pp. 2369–2375, 2006.

[18] H. S. Rad and S. Gazor, "The impact of non-isotropic scattering and directional antennas on MIMO multicarrier mobile communication channels," *IEEE Transactions on Communications*, vol. 56, no. 4, pp. 642–652, 2008.

[19] J. D. Parsons and A. M. D. Turkmani, "Characterisation of mobile radio signals: model description," *IEE Proceedings I: Communications, Speech and Vision*, vol. 138, no. 6, pp. 549–556, 1991.

[20] T. Aulin, "A modified model for the fading signal at a mobile radio channel," *IEEE Transactions on Vehicular Technology*, vol. 28, no. 3, pp. 182–203, 1979.

[21] S. Qu and T. Yeap, "A three-dimensional scattering model for fading channels in land mobile environment," *IEEE Transactions on Vehicular Technology*, vol. 48, no. 3, pp. 765–781, 1999.

[22] A. Kuchar, J.-P. Rossi, and E. Bonek, "Directional macro-cell channel characterization from urban measurements," *IEEE*

Transactions on Antennas and Propagation, vol. 48, no. 2, pp. 137–146, 2000.

[23] K. Kalliola, K. Sulonen, H. Laitinen, O. Kivekäs, J. Krogerus, and P. Vainikainen, "Angular power distribution and mean effective gain of mobile antenna in different propagation environments," *IEEE Transactions on Vehicular Technology*, vol. 51, no. 5, pp. 823–838, 2002.

[24] P. D. Teal, T. D. Abhayapala, and R. A. Kennedy, "Spatial correlation for general distributions of scatterers," *IEEE Signal Processing Letters*, vol. 9, no. 10, pp. 305–308, 2002.

[25] C. A. Balanis, *Antenna Theory: Analysis and Design*, John Wiley & Sons, New York, NY, USA, 2nd edition, 1996.

[26] H. S. Rad, S. Gazor, and P. Shariatpanahi, "Non-fixed scatterers and their effects on MIMO multicarrier fading communication channels," in *Proceedings of the 50th Annual IEEE Global Telecommunications Conference (GLOBECOM '07)*, pp. 3765–3769, Washington, DC, USA, November 2007.

[27] M. Stege, J. Jelitto, M. Bronzel, and G. Fettweis, "A multiple input-multiple output channel model for simulation of TX- and RX-diversity wireless systems," in *Proceedings of the 52nd IEEE Vehicular Technology Conference (VTC '00)*, vol. 2, pp. 833–839, Boston, Mass, USA, September 2000.

[28] S. R. Saunders, *Antennas and Propagation for Wireless Communication Systems*, John Wiley & Sons, New York, NY, USA, 1999.

[29] H. L. Bertoni, *Radio Propagation for Modern Wireless Systems*, Prentice Hall PTR, Upper Saddle River, NJ, USA, 1999.

[30] G. D. Durgin and T. S. Rappaport, "Theory of multipath shape factors for small-scale fading wireless channels," *IEEE Transactions on Antennas and Propagation*, vol. 48, no. 5, pp. 682–693, 2000.

[31] B. H. Fleury, "An uncertainty relation for WSS processes and its application to WSSUS systems," *IEEE Transactions on Communications*, vol. 44, no. 12, pp. 1632–1634, 1996.

[32] A. Algans, K. I. Pedersen, and P. E. Mogensen, "Experimental analysis of the joint statistical properties of azimuth spread, delay spread, and shadow fading," *IEEE Journal on Selected Areas in Communications*, vol. 20, no. 3, pp. 523–531, 2002.

[33] X. Zhao, J. Kivinen, P. Vainikainen, and K. Skog, "Propagation characteristics for wideband outdoor mobile communications at 5.3 GHz," *IEEE Journal on Selected Areas in Communications*, vol. 20, no. 3, pp. 507–514, 2002.

[34] G. D. Durgin, *Space-Time Wireless Channels*, Prentice Hall, Upper Saddle River, NJ, USA, 2003.

[35] T. S. Rappaport, *Wireless Communications: Principles and Practice*, Prentice Hall PTR, Upper Saddle River, NJ, USA, 1996.

[36] H. S. Rad and S. Gazor, "A 3D correlation model for MIMO non-isotropic scattering with arbitrary antenna arrays," in *Proceedings of IEEE Wireless Communications and Networking Conference (WCNC '05)*, vol. 2, pp. 938–943, New Orleans, La, USA, March 2005.

[37] H. S. Rad and S. Gazor, "Space-time-frequency characterization of 3D non-isotropic MIMO multicarrier propagation channels employing directional antennas," in *Proceedings of IEEE Wireless Communications and Networking Conference (WCNC '07)*, pp. 1888–1893, Hong Kong, March 2007.